JACS
JOURNAL OF THE AMERICAN CHEMICAL SOCIETY
Article
pubs.acs.org/JACS

Wiring of Photosystem II to Hydrogenase for Photoelectrochemical Water Splitting

Dirk Mersch,[†] Chong-Yong Lee,[†] Jenny Zhenqi Zhang,[†] Katharina Brinkert,[‡] Juan C. Fontecilla-Camps,[§] A. William Rutherford,[‡] and Erwin Reisner*[,†]

[†]Department of Chemistry, University of Cambridge, Lensfield Road, Cambridge CB2 1EW, U.K.
[‡]Department of Life Sciences, Imperial College London, London SW7 2AZ, U.K.
[§]Metalloproteins Unit, Institut de Biologie Structurale, CEA, CNRS, Université Grenoble Alpes, 38044 Grenoble, France

Supporting Information

ABSTRACT: In natural photosynthesis, light is used for the production of chemical energy carriers to fuel biological activity. The re-engineering of natural photosynthetic pathways can provide inspiration for sustainable fuel production and insights for understanding the process itself. Here, we employ a semiartificial approach to study photobiological water splitting via a pathway unavailable to nature: the direct coupling of the water oxidation enzyme, photosystem II, to the H_2 evolving enzyme, hydrogenase. Essential to this approach is the integration of the isolated enzymes into the artificial circuit of a photoelectrochemical cell. We therefore developed a tailor-made hierarchically structured indium−tin oxide electrode that gives rise to the excellent integration of both photosystem II and hydrogenase for performing the anodic and cathodic half-reactions, respectively. When connected together with the aid of an applied bias, the semiartificial cell demonstrated quantitative electron flow from photosystem II to the hydrogenase with the production of H_2 and O_2 being in the expected two-to-one ratio and a light-to-hydrogen conversion efficiency of 5.4% under low-intensity red-light irradiation. We thereby demonstrate efficient light-driven water splitting using a pathway inaccessible to biology and report on a widely applicable in vitro platform for the controlled coupling of enzymatic redox processes to meaningfully study photocatalytic reactions.

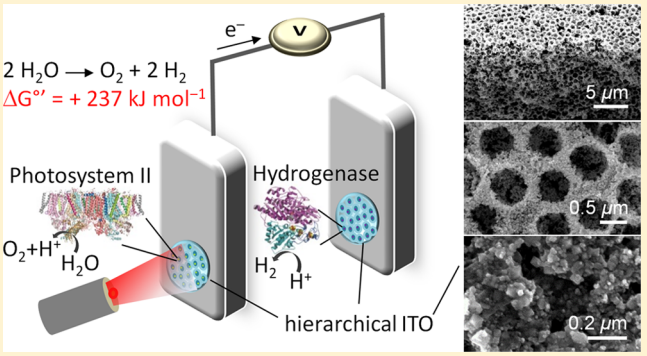

INTRODUCTION

The ability to efficiently and sustainably convert solar energy into useful chemicals such as renewable fuels (solar fuels) would pave the way for much needed renewable alternatives to fossil fuels.[1−3] Nature has evolved the ability to harness sunlight for the conversion of CO_2 and water into energy-rich compounds such as carbohydrates through photosynthesis.[4] In this process, solar energy is absorbed and used by the photosystems to remove electrons from water and to generate reducing power in the form of reduced nicotinamide adenine dinucleotide phosphate (NADPH) and a proton gradient for adenosine triphosphate (ATP) generation. These energy-rich molecules are then used to drive the "dark reactions" in the Calvin cycle, in which atmospheric CO_2 is incorporated into carbohydrates. The overall solar-to-biomass conversion efficiency of photosynthesis has been reported to be poor (<7% for cyanobacteria and <1% for crop plants).[5] Such low efficiencies (despite the presence of certain highly efficient enzymes) can be attributed to several factors. For example, CO_2 fixation is limited by the enzyme RuBisCO, which is slow and lacks substrate specificity.[6] Light absorption is noncomplementary in the light-driven enzymes, photosystem II (PSII, λ_{max} = 680 nm) and photosystem I (PSI, λ_{max} = 700 nm), which limits the wavelengths of sunlight that can be absorbed. The presence of competing light-harvesting complexes gives rise to light saturation at low light intensities and consequently low overall quantum efficiency.[5] Clearly, biological photosynthesis was evolved for biological fitness, which does not necessitate efficient chemical production.

From the viewpoint of renewable fuel generation, the capture and storage of solar energy in the form of H_2 through water splitting is more attractive than conventional biomass photosynthesis since H_2 is not only a promising future fuel, but also a key intermediate in generating carbon-based liquid fuels. Despite the presence of inefficient photosynthetic pathways, nature offers very efficient and selective enzymes for the catalysis of the solar water-splitting half-reactions, water oxidation and proton reduction, via the enzymes PSII and hydrogenase (H_2ase), respectively. PSII is a trans-membrane protein present in oxygenic photosynthetic organisms such as cyanobacteria, algae, and plants. It is responsible for the

Received: April 10, 2015
Published: June 5, 2015

DOI: 10.1021/jacs.5b03737
J. Am. Chem. Soc. 2015, 137, 8541−8549

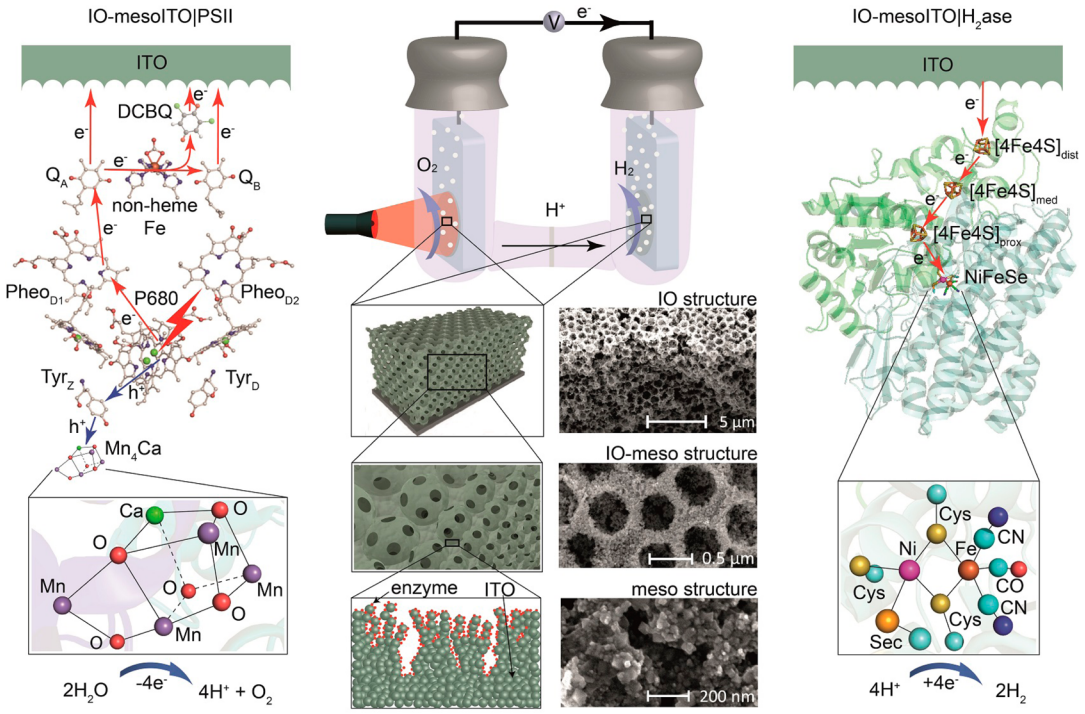

Figure 1. Schematic representation of the enzyme PEC cell. Water is photo-oxidized and O_2 is generated at the IO-mesoITO|PSII photoanode (left), and aqueous protons are reduced at the IO-mesoITO|H_2ase cathode (right). Voltage is applied between the two electrodes of the PEC cell to help drive the proton reduction reaction. The PEC cell design, the IO-mesoITO electrode architecture, and the SEM images of the IO-mesoITO electrodes are shown in the middle of the figure.

coupling of light absorption with charge separation and water oxidation catalysis, which is the first step in natural photosynthesis. It performs solar water oxidation at rates of up to 1000 s^{-1} in vivo.[7−9] H_2ases are metalloenzymes used by microbes to oxidize and produce H_2 gas at rates of up to 9000 s^{-1}.[10,11]

Extensive efforts are currently being invested to re-engineer photosynthetic organisms (e.g., green algae and cyanobacteria) for more efficient photobiological biomass and H_2 conversion. In the latter case, electrons can be diverted from CO_2 fixation for proton reduction by promoting electron transfer from the ferredoxin (following reduction by PSI) to a H_2ase.[12] However, because of the O_2 sensitivity of many H_2ases, H_2 generation occurs most readily when the water oxidation reaction involving PSII is inhibited and the electrons are derived from starch (which is synthesized during oxygenic photosynthesis).[13] As such, H_2 generation is typically transient, decoupled from O_2 generation, and overall highly inefficient (with the efficiency being extremely difficult to measure accurately).[14]

The establishment of a platform in which redox pathways/components can be selected, omitted, or rewired, with the changes to the output parameters measured, would allow for complex biological processes to be systematically and analytically dissected. For example, the coupling of PSII directly to H_2ase for light-driven water splitting was suggested[15] as a potential route to substantially enhance the biological energy conversion efficiency by eliminating many of the inefficient steps inherent to natural photobiological H_2 production. The quantitative study of this direct PSII-H_2ase pathway would give insights into the fuel conversion efficiencies achievable and give information about the current limitations arising from competing light-absorbing proteins and inefficient electron-transfer pathways in the natural system. However, this protein-engineering task is considered insurmountable using current synthetic biology approaches,[15] mainly due to the mismatched reduction potentials of the terminal hydroquinone of PSII with the iron−sulfur clusters of H_2ase.

Here, we report an in vitro platform to directly couple PSII to H_2ase to study photobiological water splitting for simultaneous O_2 and H_2 evolution. Our approach involves the integration of the selected enzymes into a two-compartment photoelectrochemical (PEC) cell, where oxygenic and anaerobic reactions can be separated and an external bias can be applied to study the additional energy that is needed to drive the overall photoreaction. Key to the reliable quantification of the output parameters is the ability of the electrodes to immobilize sufficient amounts of redox enzymes in electroactive configurations. We have therefore developed a hierarchically structured indium−tin oxide (ITO) electrode, which gives rise to exceptionally high loadings of both PSII and H_2ase and facilitates efficient photo-oxidation of water and proton reduction activities, respectively.

RESULTS

Tailor-Made Electrodes for the Integration of Redox Enzymes. PSII dimers isolated from *Thermosynechococcus elongatus* (approximately 10.5 × 20.5 × 11.0 nm^3 or 700 kDa in size, Figure 1, left)[16] and a [NiFeSe]-H_2ase isolated from *Desulfomicrobium baculatum* (approximately 7.2 × 7.8 × 6.0 nm^3 or 86 kDa in size, Figure 1, right)[17] were employed in this study and selected based on their suitability for use in water splitting (see below). ITO electrodes with a macroporous inverse opal (IO) architecture and a mesoporous skeleton (this electrode will henceforward be denoted as "IO-mesoITO") were specifically developed for the integration of these enzymes (Figure 1, center). ITO was selected as the electrode material due to its known transparency and conductivity.[18] Macro-

DOI: 10.1021/jacs.5b03737
J. Am. Chem. Soc. 2015, 137, 8541−8549

porous features were introduced to facilitate the penetration of the enzymes, substrates, and products throughout the electrode structure. A mesoporous ITO skeleton was incorporated to further increase the effective surface area for enzyme interactions and to facilitate stable anchoring, as well as electronic coupling by providing multiple connection points between the enzyme and ITO surface. Light scattering is also promoted within the IO-mesoITO structure due to the disorganized nature of the chambers; this increases the effective light path length and facilitates photoabsorption by the embedded PSII.[19]

Hierarchical IO-mesoITO was assembled using a colloidal coassembly approach that utilized polystyrene beads (750 nm diameter) and ITO colloids (<50 nm diameter; Supporting Information Figure S1). Following sintering, a mesoporous ITO skeleton is formed around the macroporous IO chambers, derived from the decomposition of the organic polystyrene template. This approach gives rise to interconnected macro-chambers with a diameter of approximately 750 nm and 150 nm wide connecting channels. The pore sizes of the mesoporous features were up to 50 nm in diameter (Figure 1, center). IO-mesoITO films of up to 80 μm in thickness can be assembled using this method (Supporting Information Figure S2). X-ray diffractometry confirmed the composition of the electrode to be free from contamination and chemical alterations (Supporting Information Figure S3). By varying the amount and dimensions of the polystyrene and ITO colloids, the dimensions of the macro/meso pores and the film thickness can be tuned, and this type of electrodes can be further customized for the integration of a wide range of enzymes and biological materials.

This hierarchically structured electrode exhibited substantial improvements in enzyme adsorption compared to those observed for flat and mesoporous electrodes, which are commonly employed in protein film electrochemistry.[20−22] The optimized enzyme−IO-mesoITO electrodes gave rise to high photocurrents, which allowed for the gaseous products to be quantified. This was previously not possible due to the generation of products being below the limit of detection (in particular for PSII), and the light- and current-to-product conversion efficiencies (faradaic yield) reported in protein film electrochemistry had typically relied on the assumption of 100% conversion.[21,23] IO electrode architectures have been used in devices for over a decade, but have been generally utilized for their photonic properties[24−26] and less so for their high surface area.[27] IO and other nanostructured metal oxide electrodes have recently been reported for the adsorption of small proteins such as cytochrome *c*.[28−31] However, these IO electrodes require a more complicated preparation procedure and the maximum thicknesses that have been achieved are more than 1 order of magnitude thinner (<2.5 μm) than the tailored electrodes reported here. Such dimensions limit the ability of the electrode to support the enzyme loading capacity required for product quantification. The thickness of our IO-mesoITO electrodes overcomes this hurdle and enables accurate determination of the final conversion efficiency achieved in enzyme PEC cells.

Photoelectrochemical Water Oxidation by Photosystem II. *T. elongatus* PSII was chosen mainly for its relative robustness,[7,32] and the PSII in this study needs only to sustain photo-oxidation of water long enough for product quantification (<1 h). To construct the PSII electrode for protein film PEC (PF-PEC) studies,[7] PSII was drop-cast onto IO-mesoITO

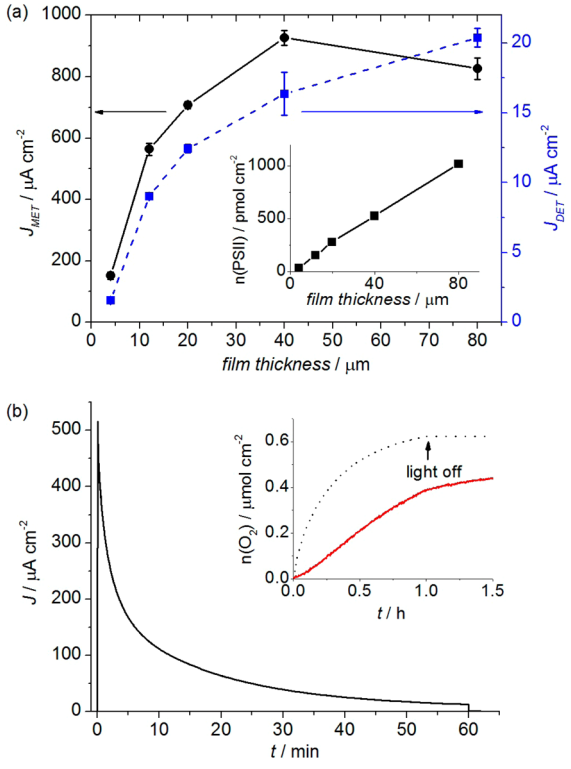

Figure 2. PF-PEC response of the IO-mesoITO|PSII photoanode. (a) Photocurrents generated by DCBQ-mediated (MET) and direct electron transfer (DET), as a function of the IO-mesoITO film thickness in a pH 6.5 electrolyte solution. Inset shows the maximum loading of PSII on the electrode as a function of the IO-mesoITO electrode thickness. IO-mesoITO|PSII electrodes were irradiated with λ = 679 nm and I = 10 mW cm^{-2} at an applied potential of 0.5 V vs NHE. (b) Photocatalytic stability of IO-mesoITO|PSII electrode (20 μm film thickness). Inset shows the comparison of the theoretical (dashed trace), based on 100% faradaic yield, and experimental (solid trace) O_2 production. IO-mesoITO|PSII electrodes were irradiated with λ = 660 nm and I = 10 mW cm^{-2} under continuous stirring at an applied potential of 0.5 V vs NHE.

and allowed to adsorb in the dark for up to 15 min. Subsequently, the IO-mesoITO|PSII electrode was rinsed with the electrolyte solution to remove the nonadsorbed and excess enzymes before use in PF-PEC studies. Figure 2a shows the maximum loading capacity and PF-PEC response of PSII on an IO-mesoITO electrode as a function of the ITO film thickness. The PSII loading increased linearly from 36 ± 3 to 1020 ± 11 pmol cm^{-2} when the film thickness was increased from 4 to 80 μm; this compares favorably to previously reported electrodes where maximum PSII loadings of up to 76 pmol cm^{-2} were recorded.[7]

The favorable interaction of PSII with mesoporous ITO was previously established, and an onset of photoanodic current at 0.2 V versus NHE with a saturation photocurrent at 0.5 V versus NHE with <2 μA cm^{-2} was observed in a pH 6.5 electrolyte solution in the absence of a redox mediator.[7,21] In this study, illumination of the IO-mesoITO|PSII electrode with red light (λ = 679 nm, I = 10 mW cm^{-2}) generated a much larger photocurrent at an applied potential of 0.5 V versus NHE (Figure 2 and Supporting Information Figure S4). Photocurrent generation is triggered by excitation of the P680 cluster of chlorophylls *a* (Chl *a*) in the PSII reaction center, which generates a radical pair consisting of a Chl *a* cation and a

DOI: 10.1021/jacs.5b03737
J. Am. Chem. Soc. 2015, 137, 8541−8549

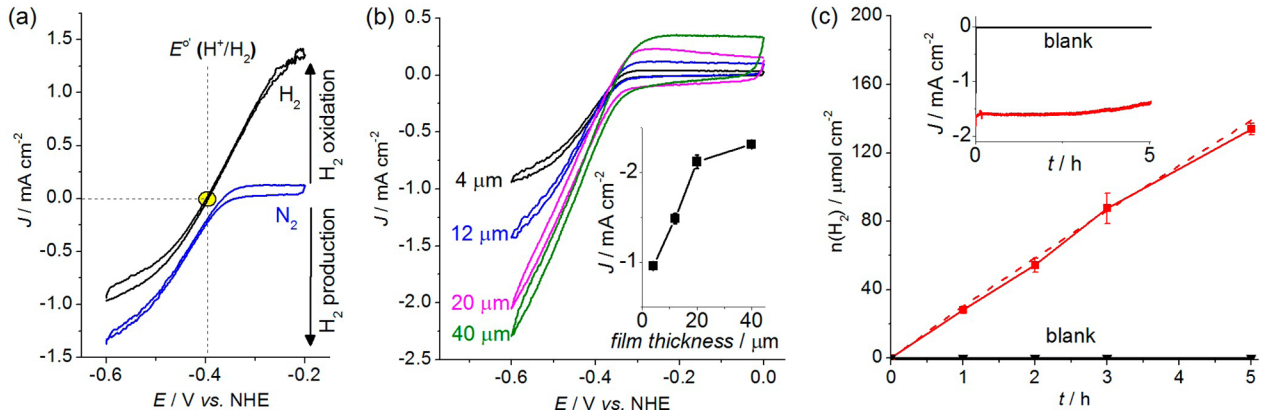

Figure 3. Electrocatalytic response of the IO-mesoITO|H_2ase electrode. (a) Protein film voltammograms in a stirred pH 6.5 electrolyte solution under an atmosphere of 100% N_2 and 100% H_2 (1 bar). (b) Voltammograms showing the electrocatalytic response for proton reduction with different IO-mesoITO film thicknesses at pH 6.0 under N_2. Inset shows the catalytic current at −0.6 V vs NHE as a function of IO-mesoITO film thickness. (c) Comparison of measured (solid trace) and theoretical (dashed trace) H_2 production based on 100% faradaic yield at −0.6 V vs NHE (η = 246 mV) at pH 6.0. Inset shows the corresponding CPE traces. Blank experiments in the absence of H_2ase are also shown. The IO-mesoITO|H_2ase electrodes had a geometrical surface area of 0.25 cm^2, and all experiments were performed at room temperature. An IO-mesoITO film thickness of 12 μm was used in panels a and c, and a scan rate of 10 mV s^{-1} in panels a and b.

pheophytin anion (Figure 1). The Chl *a* cation oxidizes a tyrosine side chain, which acts as a relay to oxidize the Mn_4Ca active site for water oxidation to O_2. The pheophytin anion reduces the plastoquinone Q_A, which acts as electron relay to reduce the mobile electron acceptor plastoquinone Q_B.[33] In the absence of a Q_B pool in the artificial setting, Q_B may be lost and electron transfer would occur directly from Q_A to the ITO if it is close enough to the metal oxide surface,[21] or indirectly via a soluble redox mediator that is analogous to Q_B, such as 2,6-dichloro-1,4-benzoquinone (DCBQ; midpoint redox potential E_m = 0.36 V vs NHE, Supporting Information Figure S5).[7,21] In the presence of excess DCBQ, a remarkably high mediated electron-transfer (MET) photocurrent of 930 ± 30 μA cm^{-2} (Figure 2a) with a corresponding external quantum efficiency (EQE) of (17.0 ± 0.5)% (calculated using eq 1 in the Experimental Section) was recorded with IO-mesoITO|PSII (40 μm film thickness). The EQE of less than 100% implies that the integration of PSII into the PF-PEC system can be further improved to enhance performance. In the absence of a mediator, a maximum direct electron-transfer (DET) photocurrent of 20 ± 1 μA cm^{-2} was observed with IO-mesoITO|PSII (80 μm film thickness). These MET and DET photocurrent densities are the highest reported to date with PSII electrodes.[7] Previously, benchmark photocurrents of 45 μA cm^{-2} were reported, which were too low for O_2 detection.[20] The apparent saturation in photocurrent arising from electrodes thicker than 40 μm can be attributed to increasing resistance, mass transport limitations, and light screening by the thicker layers.

Photocurrent generation by PSII at the anode was coupled to O_2 evolution and the release of protons, which could then diffuse to the cathode. The high photocurrents generated by the IO-mesoITO|PSII electrode gave rise to quantifiable amounts of O_2 gas. Controlled potential electrolysis (CPE) carried out using IO-mesoITO|PSII in the presence of DCBQ during red-light irradiation for 1 h at an applied potential of 0.5 V versus NHE resulted in the passage of 0.23 ± 0.01 C cm^{-2} of charge and the generation of 0.45 ± 0.01 (μmol O_2) cm^{-2} as quantified by a fluorescence-based O_2 sensor (Figure 2b). This corresponds to a faradaic yield of (75 ± 4)%, a PSII-based turnover number (TON_{PSII}) of 4200 ± 200 (mol O_2) (mol PSII)$^{-1}$ and an initial turnover frequency (TOF_{PSII}) of 12.9 ± 0.4 (mol O_2) (mol PSII)$^{-1}$ s^{-1} (calculated using eq 2 in the Experimental Section). O_2 measurements were also performed at the end of the CPE experiments using gas chromatography with O_2 levels of 0.52 ± 0.05 (μmol O_2) cm^{-2} being detected in the headspace. The photocurrent generated by IO-mesoITO|PSII decayed to a few percent of its initial value within 1 h, and this photoinstability can be attributed to photodamage of PSII, which is the limiting factor in the full water-splitting cell, see below. Supporting Information Figure S6 shows control PEC experiments conducted with and without immobilized PSII. In a control experiment where PSII was added to the electrolyte solution instead of being immobilized onto the electrode, negligible photocurrents were observed in the presence of DCBQ during 30 s of irradiation. This observation can be attributed to mass transport limitations associated with the DCBQ in the bulk solution reaching the electrode surface, thereby significantly hindering electron injection into the electrode.

Electrochemical H_2 Evolution by Hydrogenase. Our semiartificial approach to water splitting allows selecting a suitable H_2ase for this purpose. *D. baculatum* [NiFeSe]-H_2ase was chosen for its high proton reduction activity, tolerance toward O_2, and negligible product inhibition by H_2.[34,35] Thus, [NiFeSe]-H_2ase allows for the efficient formation and accumulation of H_2 during the water-splitting process, where O_2 is also generated as a byproduct.[36]

[NiFeSe]-H_2ase was drop-cast onto the IO-mesoITO electrode, and excess H_2ase removed by rinsing with the electrolyte solution before being used in electrochemical studies. The electrocatalytic response of *D. baculatum* [NiFeSe]-H_2ase on the IO-mesoITO electrode under different conditions is summarized in Figure 3 and Supporting Information Figure S7. Protein film voltammetry with IO-mesoITO|H_2ase was performed at a scan rate of 10 mV s^{-1} at pH 6.5 under stirring and a H_2 atmosphere. Interfacial electronic communication occurs between ITO and the distal [4Fe4S] cluster in the small subunit, and catalytic turnover proceeds at the [NiFeSe]-active site in the large subunit of the enzyme (Figures 1 and 3a).[37] The electrocatalytic reversibility corresponding to the interconversion of protons to H_2 and the

DOI: 10.1021/jacs.5b03737
J. Am. Chem. Soc. 2015, 137, 8541−8549

high current densities generated demonstrate that the H_2ase was efficiently wired to the ITO. ITO is therefore a suitable electrode material for [NiFeSe]-H_2ases, and the IO-mesoITO|H_2ase electrode gave rise to substantially higher current densities for H_2 evolution than that of previously used electrode materials (<200 μA cm^{-2}).[35,38] Only a marginal overpotential from $E^{0\prime}(H^+/H_2)$ of −0.395 V versus NHE (pH 6.5) is required for proton reduction and H_2 oxidation. The protein film voltammogram also confirms that the enzyme exhibited excellent H_2 evolution activity with negligible inhibition by its product, H_2. Under a N_2 atmosphere, an onset potential of −0.35 V versus NHE (pH 6.5) is required to initiate catalytic proton reduction. The electrocatalytic currents generated by the IO-mesoITO|H_2ase electrodes increased with the ITO film thickness and reached saturation at a thickness of 20 to 40 μm (Figure 3b). The high catalytic currents for proton reduction obtained using IO-mesoITO|H_2ase indicate that the use of soluble redox mediators is unnecessary to keep up with the electron flow from the PSII photoanode.

CPE was performed on IO-mesoITO|H_2ase at an applied potential of −0.6 V versus NHE at pH 6.0 (Figure 3c). After 5 h of CPE, at least 80% of the high initial current remained, a charge of 27 ± 1 C cm^{-2} had passed through the external circuit, and 134 ± 4 (μmol H_2) cm^{-2} were measured in the headspace by gas chromatography, which corresponds to a faradaic yield of (96 ± 3)%. High currents and faradaic yields of (88 ± 2)% and (92 ± 2)% were also observed at an applied potential of −0.5 and −0.4 V after 5 h of CPE, respectively (Supporting Information Figure S8). This indicates that IO-mesoITO is an excellent electrode material up to an applied potential of −0.6 V versus NHE (note that at a lower potential, degradation of ITO occurs).[39]

Previously, the performance of H_2ase in protein film electrochemistry has been largely limited by poor enzyme integration at the electrode.[22] Despite significant advancements, such as the use of nanostructured carbon-based electrodes to enhance catalytic currents for the H_2 oxidation reaction,[40−42] electrodes that can support high and stable enzyme loading for the electrocatalytic proton reduction reaction are rare.[43] Attempts to improve the stability of the protein film included the covalent attachment of H_2ase to functionalized pyrolytic graphite electrodes[44] and the use of metallic single-wall carbon nanotubes/carbon cloth[45] and carbon felt.[43] These gave rise to high loadings of the enzyme; however, the stability of the enzyme−electrode interaction was highly variable. The IO-mesoITO electrode used in this study demonstrated both high loading and stable integration of the H_2ase.

PEC Full Water Splitting. To establish the external bias needed to drive a two-electrode system for light-induced water splitting (ΔE^0 = 1.23 V; ΔG^0 = 237.2 kJ mol^{-1}), the onset photoanodic potential of the mediated IO-mesoITO|PSII electrode system during red-light irradiation and the onset cathodic potential of the IO-mesoITO|H_2ase electrode obtained from the three-electrode system were compared (Figure 4a). The onset of the cathodic current is fixed by $E^{0\prime}(H^+/H_2)$, whereas the half-wave potential of the anodic photocurrent is approximately equal to the E_m of the DCBQ mediator. Hence, it can be predicted that a bias potential of at least 0.6 V is required for the combined cell to perform light-driven water splitting in a two electrode configuration. An additional driving force will be needed to generate an observable amount of current and to overcome any uncompensated solution resistance. The cathodic current is

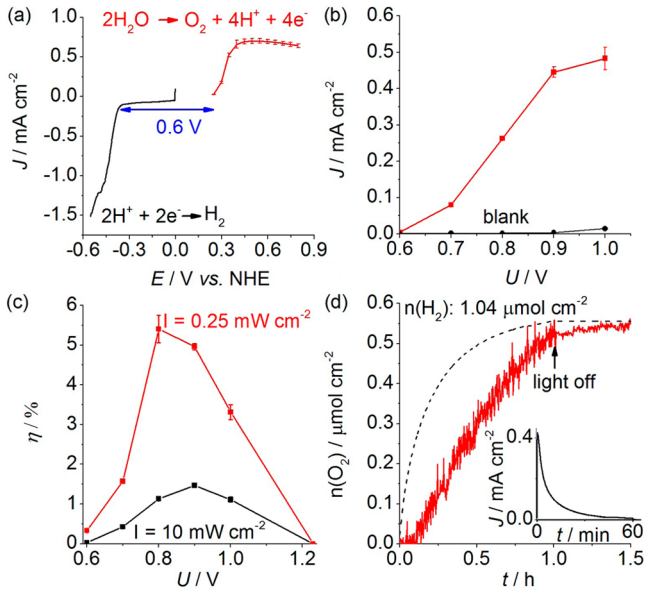

Figure 4. Characterization of the PEC water-splitting cell. (a) Voltammogram recorded with an IO-mesoITO|H_2ase electrode (12 μm thick, ν = 5 mV s^{-1}, black trace) and the mediated photocurrents of an IO-mesoITO|PSII electrode (20 μm thick, red trace, λ = 660 nm illumination at 10 mW cm^{-2}) in a three-electrode configuration. (b) Photocurrent response in a two-electrode PEC cell during red-light irradiation with mediated IO-mesoITO|PSII wired to IO-mesoITO|H_2ase (both electrodes as described in panel a) as a function of applied voltage (red trace). A control experiment in the absence of H_2ase is also shown (black trace). (c) Light-to-hydrogen conversion efficiency (η) of PEC cell with the mediated IO-mesoITO|PSII electrode of 20 μm thickness, irradiated with 10 mW cm^{-2} intensity (λ = 660 nm, black trace), or 40 μm thickness at 0.25 mW cm^{-2} (red trace) in combination with a 12 μm thick IO-mesoITO|H_2ase electrode. (d) Theoretically produced O_2 based on charge collected during CPE (black dashed trace; expressed in μmol O_2 per cm^2 of geometrical IO-mesoITO surface area) and the experimentally measured O_2 (red trace) in the two-electrode PEC system with mediated IO-mesoITO|PSII and IO-mesoITO|H_2ase with an applied voltage of U = 0.9 V during continuous λ = 660 nm irradiation at 10 mW cm^{-2}. Inset: photocurrent density generated during the experiment. All experiments were performed at room temperature and the electrodes had a geometrical surface area of 0.25 cm^2.

higher than the anodic photocurrent, which indicates that the anodic component will be the limiting half-reaction in the PEC cell.

The mediated IO-mesoITO|PSII photoanode system (20 μm thick) was wired to the IO-mesoITO|H_2ase (12 μm thick) cathode in a two-compartment cell separated by a glass frit (Supporting Information Figure S9). Separation of the cathodic and the anodic reaction minimizes the exposure of H_2ase to O_2 at the time of PSII activity, which would be very difficult to achieve in in vivo systems. As predicted, photocurrents were generated at an applied voltage (U) of more than 0.6 V. A current density of 450 ± 10 μA cm^{-2} was observed at U = 0.9 V, which corresponds to a light-to-hydrogen conversion efficiency of (1.5 ± 0.1)% (λ = 660 nm, I = 10 mW cm^{-2}; calculated using eq 3 in the Experimental Section; the applied bias was accounted for, see Figure 4, parts b and c). The efficiency was further optimized by reducing the irradiation intensity to 0.25 mW cm^{-2} and utilizing thicker IO-mesoITO|PSII electrodes (40 μm) for higher PSII loading. Under these

DOI: 10.1021/jacs.5b03737
J. Am. Chem. Soc. 2015, 137, 8541−8549

conditions, the light-to-hydrogen conversion efficiency reached a maximum of (5.4 ± 0.3)% at U = 0.8 V.

After 1 h of continuous red-light irradiation (I = 10 mW cm^{-2}) at an applied voltage U of 0.9 V, the PEC cell generated 0.20 ± 0.02 C cm^{-2} of charge, 0.52 ± 0.04 (μmol O_2) cm^{-2}, and 0.96 ± 0.08 (μmol H_2) cm^{-2}, which corresponds to a faradaic yield of (104 ± 5)% and (98 ± 2)%, respectively (Figure 4d). In control experiments where electrodes without adsorbed PSII or H_2ase were examined, negligible photocurrents were detected (Supporting Information Figure S10).

DISCUSSION

The hierarchical IO-mesoITO electrodes reported here represent a significant advancement in bioelectrode design, and gave rise to unprecedented photocurrent densities generated by a PSII photoanode, and excellent activity and stability exhibited by the H_2ase cathode. This in turn allowed for O_2 evolution by PSII and H_2 production by H_2ase to be quantified and thus meaningfully studied in a combined PEC system. Output parameters, including faradaic efficiencies and light-to-hydrogen conversion efficiencies under different conditions, could thus be experimentally determined for the first time. In this case, light-induced water splitting was demonstrated at an electrochemical bias below its thermodynamic potential, and H_2 and O_2 generation was detected in the expected stoichiometric two-to-one ratio. An efficiency of up to 5.4% was achieved under low-intensity red-light irradiation (with the electrical bias accounted for), demonstrating that light energy can be converted and stored efficiently as a chemical fuel via this pathway. Our proof-of-principle PEC system thereby demonstrates that an endergonic and novel photobiological H_2 production pathway can be studied, which cannot be accessed using in vivo methods. The half-reactions can be further systematically assessed individually to determine limiting factors, which will lead to improvements to the overall system. In this case, the limiting factor is the PSII photoanode with respect to photocurrent density, onset potential, and long-term-stability. It should be noted that the efficiency achieved by this PEC setup cannot account for the additional energy that is stored when charges are transported across the thylakoid membrane in the light-dependent reaction of biological photosynthesis.

Currently, the light-to-hydrogen conversion efficiency of this system has only been optimized for a red-light-absorbing system. An additional bias is still needed to drive the complete reaction, which results in suboptimal energy storage. The required bias potential of U > 0.6 V can in principle be reduced to some extent by selecting different mediators with a more negative E_m or by extracting electrons at an earlier electron-transfer step such as at the reduced Pheo or Q_A, which have a greater reducing potential than the Q_B.[7,21,46] Accessing the Pheo would be difficult; however, a better control of the enzyme orientation and improvements to the PSII−electrode interface such that the Q_A is closer to the electrode surface for direct electron injection may help to eliminate the need for diffusional quinone mediators. Future studies will also work toward a tandem cell strategy through the photosensitization of the anode or cathode.[34] This could involve the use of an appropriate semiconductor or dye such that energy can be harnessed from regions of the solar spectrum complementary to those of the PSII Chl *a* to provide the electrons delivered from PSII quinones with greater reducing power.

The proof-of-principle enzyme-based PEC cell presented here demonstrates that energy can be chemically stored, even with the application of an external bias, by the rational wiring of appropriate enzymes. Our enzyme PEC system is different from previously reported PEC systems, where only exothermic or close to energy neutral reactions were catalyzed by a pair of heterogenized enzymes. For example, a H_2 fuel cell was assembled by the coupling of a *Ralstonia eutropha* [NiFe]-membrane bound H_2ase to a laccase from *Trametes versicolor*, which catalyzed the highly exergonic reverse reaction of water splitting.[47] Direct coupling of the H_2ase Hyd-2 from *Escherichia coli* to a carbon monoxide dehydrogenase (CODH I) from *Carboxydothermus hydrogenoformans* on a graphite particle allowed for the slightly exergonic water gas shift reaction to be catalyzed (ΔG^0 = −28.6 kJ mol^{-1}).[48] Another notable example includes a PEC system that coupled a PSII electrode to a PSI electrode to mimic the Z-scheme in photosynthesis. Water oxidation to O_2 at the anode was counteracted with the reduction of O_2 to water at the cathode to result in production of electricity.[49] Light-driven H_2 production using H_2ase has been achieved in the past in combination with light harvesting materials, but only in the presence of a sacrificial electron donor.[38,43,50,51] Complete light-driven water splitting containing a H_2ase-based half reaction had not previously been reported in vitro.

CONCLUSIONS

Despite the relatively poor efficiency of photobiological H_2 production in vivo, nature provides us with highly active and abundant enzymes that are much more efficient in performing solar water splitting than any low-cost synthetic catalysts. The reported semiartificial PEC platform allows us to select efficient biological elements (such as the fuel-producing enzymes PSII and H_2ase) and eliminate inefficient photosynthetic steps (such as unsuitable metabolic pathways) by wiring the isolated enzymes together in a PEC cell. This approach permits specific catalytic processes to be studied rationally and systematically, and reveals limiting parameters, which are difficult to investigate in biological systems.

As an example, this study explored an unnatural photobiological H_2 production pathway to understand how an existing reaction pathway can be "rewired" to increase light-to-hydrogen conversion efficiencies. The reported enzyme hybrid cell shows red-light-driven water splitting at an electrochemical bias below its thermodynamic potential and H_2 and O_2 production separated in two compartments in the expected stoichiometric two-to-one ratio, yielding a light-to-hydrogen conversion efficiency of up to 5.4%. The direct coupling of PSII to H_2ase was therefore revealed to be an efficient route, and further improvements in the light-to-product conversion efficiencies are expected to accompany further improvements to the PSII−photoanode interface. The quantification of the PEC output parameters was made possible in this study by the advancements made in electrode design, which allow for excellent enzyme integration. The hierarchical macro−mesoporous ITO electrode structure reported in this study can be readily adapted to host different guest materials for a range of other applications.

EXPERIMENTAL SECTION

Materials. All chemicals, 2,6-dichloro-1,4-benzoquinone (DCBQ, Sigma-Aldrich), 2-(*N*-morpholino)ethanesulfonic acid (MES, Alfa Aesar), tris(hydroxymethyl)amino-methane (Tris, Sigma-Aldrich),

DOI: 10.1021/jacs.5b03737
J. Am. Chem. Soc. 2015, 137, 8541−8549

$CaCl_2$ (Breckland Scientific), $MgCl_2$ (Fisher Scientific), KCl (Alfa Aesar), glycerol (VWR Chemicals), KOH (Breckland Scientific), betaine (Fisher Scientific), NH_4OH (30%) solution (Fisher Scientific), H_2O_2 (30%) solution (Fisher Scientific), polystyrene beads (Polysciences, Inc.), ITO nanoparticles (Sigma-Aldrich), and fluoride-doped tin oxide (FTO)-coated glass (Sigma-Aldrich), were purchased from commercial suppliers and used without further purification unless otherwise noted. Reagents for the analytical part of the work were of the highest available purity.

The following aqueous pH 6.5 electrolyte solution was employed for the PF-PEC experiments with PSII: $CaCl_2$ (20 mM), $MgCl_2$ (15 mM), KCl (50 mM), and MES (40 mM). Glycerol (5%) was added, and no $MgCl_2$ and KCl were used for experiments studying the photocurrent response versus the film thickness of IO-mesoITO|PSII. DCBQ in DMSO was added to the PEC cell for mediated photocurrent measurements to give a final concentration of 1 mM. For H_2ase experiments in a three-electrode configuration, an aqueous MES solution (50 mM) was used. PEC water-splitting experiments were performed in an electrolyte solution at pH 6.5 containing MES (40 mM), $CaCl_2$ (20 mM), KCl (50 mM), and $MgCl_2$ (15 mM).

Isolation and Purification of Enzymes. [NiFeSe]-hydrogenase from *D. baculatum* (H_2ase) was purified using a previously published method.[52] The pure enzyme was dialyzed against 20 mM Tris/HCl at pH 7.6. The enzyme integrity was verified spectrophotometrically at λ = 604 nm by measuring its specific activity for H_2 oxidation with an aliquot of the H_2ase under H_2 in the presence of methyl viologen (1 mM) for 30 min at 30 °C. The preparation has a specific activity of 2115 μmol H_2 min^{-1} mg^{-1}, and the stock enzyme solution was diluted with 20 mM Tris/HCl buffer in an anaerobic glovebox to obtain a concentration of 8 μM before adsorption on the electrodes.

Photosystem II core particles were isolated from a CP47 His-tagged mutant from the thermophilic cyanobacterium *T. elongatus* BP-1 by Ni^{2+}-affinity chromatography as described previously, resulting in PSII at 2−3 mg of chlorophyll mL^{-1}.[32,53] The same buffers and procedures were used but with the following minor modifications: the medium was supplemented with 10 mM bicarbonate instead of being bubbled with CO_2, and a light intensity of 40 μE m^{-2} s^{-1} was used. The cells were harvested using a cell concentrator (Watson-Marlow Pumps Group), followed by centrifugation and washing in a "PSII buffer" containing MES (40 mM, pH 6.5), $MgCl_2$ (15 mM), $CaCl_2$ (15 mM), glycerol (10%), and betaine (1 M). The cells were ruptured by passing the suspension twice through a chilled cell disruptor (Constant Systems, model T5) at 25 kpsi. Oxygen evolution activity was assayed with a Clark-type O_2 electrode (Oxylab, Hansatech) in the presence of DCBQ (0.5 mM) and potassium ferricyanide (1.0 mM) at 25 °C using saturating red light (590 nm cutoff filter; 13 000 μE m^{-2} s^{-1}). The activity was determined to be about 3500 μmol O_2 mg (Chl *a*)$^{-1}$ h^{-1} under these conditions.

Physical Characterization. The surface morphology of the electrodes was analyzed by scanning electron microscopy (SEM; Philips XL30). Feature dimensions have been measured by built-in software. Powder X-ray diffraction (XRD) analysis was carried out using an X'Pert PRO X-ray diffractometer (PANalytical B.V., The Netherlands). UV−vis absorption spectra were recorded on a Varian Cary 50 UV−vis spectrophotometer (Agilent Technologies). A 5804 Eppendorf centrifuge was used, and a Carbolite furnace (ELF 11/14B/301) was used to anneal the electrodes.

An Agilent 7890A series gas chromatograph equipped with a 5 Å molecular sieve column and N_2 carrier gas was employed for the quantification of H_2. Quantification of O_2 was performed inside an MBraun glovebox to avoid leakage of atmospheric O_2 with a calibrated fluorescence-based O_2 sensor (Neofox with an Ocean Optics FOSPHOR probe). The probe was protected from direct irradiation, the background signal was subtracted from all measurements, and the reported O_2 values were corrected for dissolved oxygen using Henry's Law. A lag phase in the O_2 measurement could be observed at the start of the irradiation period due to the time required for dissolved O_2 in solution to reach the sensor positioned in the headspace of the PEC cell. The final O_2 readings from the fluorescence sensor were verified by gas chromatography (He carrier gas) for the three-electrode CPE experiments.

Preparation of IO-mesoITO electrodes. A mixed dispersion of ITO nanoparticles (<50 nm diameter) and polystyrene beads (750 nm diameter, 2.54% w/v suspension in water) was prepared as follows: ITO nanoparticles (35 mg) were dispersed by sonication in a MeOH/water (6:1 v/v) mixture (300 μL) for 3 h. The dispersion of polystyrene beads (1 mL) was centrifuged, the supernatant removed, and the polystyrene pellet redispersed in MeOH (1 mL). The polystyrene dispersion was centrifuged again, the supernatant removed, and the dispersion of ITO nanoparticles added to the polystyrene pellet. This mixture was thoroughly vortexed and sonicated for 5 min in ice cold water (<5 °C) to give the polystyrene−ITO dispersion.

FTO-coated glass (8 Ω cm^{-2}) was sonicated in isopropyl alcohol and ethanol and stored at 150 °C. A Parafilm ring was placed onto FTO to define the geometrical surface area for the IO-mesoITO films, and the polystyrene−ITO dispersion was drop-cast onto this predefined area. An amount of 4.2 μL of the described polystyrene−ITO dispersion on a 0.25 cm^2 geometrical surface area corresponds to a 10 μm thick IO-mesoITO structure. If higher film thicknesses were desired, polystyrene−ITO mixture was deposited several times with at least 4 h drying period in between. The electrodes were heated with 1 °C min^{-1} from room temperature to 500 °C and annealed at this temperature for 20 min. The IO-mesoITO electrodes were cleaned by placing them in a mixture of 30%H_2O_2/H_2O/30%NH_4OH (1:5:1 v/v) at 70 °C for 15 min, rinsed with water, and heated for 1 h at 180 °C to give a contamination-free hydrophilic ITO surface.

Deposition of Enzymes onto IO-mesoITO Electrodes. A fresh aliquot of frozen PSII was thawed for use in each experiment. It was determined that the enzyme saturation occurred at 3.2 pmol of PSII per 1 μm of IO-mesoITO film thickness (geometrical surface area: 0.25 cm^2). At least 150% of this amount of PSII was drop-cast onto the electrode to ensure enzyme saturation on the electrode when varying the film thickness. A stock PSII solution contained 2.4 mg Chl *a* mL^{-1} (77 μM of PSII). A standard film thickness of 20 μm was used for the IO-mesoITO|PSII electrode, unless otherwise stated. The amount of PSII on the IO-mesoITO surface was quantified by scratching the IO-mesoITO off the substrate after PEC experiment and into a centrifuge vial using MeOH (0.5 mL). The vial was centrifuged for 1 min at 10 000 rpm, and a UV−vis spectrum of the MeOH supernatant was recorded. The band with an absorption maximum of λ_{max} = 665 nm is assigned to Chl *a* (extinction coefficient ε = 79.95 (Chl *a* mg)$^{-1}$ mL cm^{-1}) and was used to calculate the amount of PSII monomers assuming that each PSII monomer contains 35 Chl *a* molecules.[21]

The diluted H_2ase solution (8 μM, in 20 mM Tris/HCl buffer, pH 7.0) was stored in small volume vials at −30 °C and thawed immediately before use. The H_2ase solution was drop-cast onto the cleaned IO-mesoITO electrodes (geometrical surface area of 0.25 cm^2) and allowed to dry. The loading of H_2ase was adjusted accordingly depending on the electrode thickness (6 pmol of H_2ase per 1 μm of film thickness). A standard film thickness of 12 μm was used for the IO-mesoITO|H_2ase electrode, unless otherwise stated.

Electrochemical Studies. All electrochemical experiments were performed with an Ivium Compactstat potentiostat/galvanostat at 22−25 °C. Stationary working electrodes were employed, and the electrolyte solution was stirred during all measurements to enhance convection, apart from the IO-mesoITO|PSII thickness versus photocurrent study. Protein film voltammetry and CPE were performed in a three-electrode configuration with the IO-mesoITO working electrode located in the same compartment as the Ag/AgCl (3 M NaCl) (Bioanalytical Systems) reference electrode, and the platinum counter electrode in the other compartment. All redox potentials are quoted against the normal hydrogen electrode (NHE), and the potentials were obtained by using the following correction factor: $E_{NHE} = E_{Ag/AgCl} + 0.209$ V.

Experiments with PSII were either conducted under air (studies of the photocurrent responses vs different film thicknesses of IO-mesoITO|PSII in a three-electrode system) or in an MBraun glovebox (all other measurements; O_2 concentration of less than 1 ppm). A light

DOI: 10.1021/jacs.5b03737
J. Am. Chem. Soc. 2015, 137, 8541−8549

source (Kodak S-AV 2000) with a halogen lamp was employed in all PEC experiments outside the glovebox. The light was collimated by a plano-convex lens and filtered by a band-pass filter (679 nm; full width at half-maximum, 10.3 nm). The light intensity was adjusted to 10 mW cm^{-2}. Inside the glovebox, an Ivium modulight LED module with λ = 660 nm wavelength and an adjusted intensity of 10 or 0.25 mW cm^{-2} was employed. The following procedure was used for the determination of the PEC photocurrent response of IO-mesoITO|PSII at 0.5 V versus NHE: the working electrode was exposed to continuous 30 s dark and 30 s red-light exposure cycles. A total of three cycles were recorded, and the photocurrent response (I_{Ph}) was defined as the final photocurrent after the third light exposure (Supporting Information Figure S4). After recording the nonmediated photocurrent, DCBQ was added for mediated photocurrent measurements. All experiments involving the H_2ase were carried out in the MBraun glovebox.

For PEC water splitting, a gas tight two-electrode two-compartment cell was employed with IO-mesoITO|PSII separated from IO-mesoITO|H_2ase by a glass frit in an aqueous pH 6.5 electrolyte solution. The O_2 concentration in the anodic compartment was continuously monitored by a fluorescence probe, and the H_2 was quantified in the headspace of the cathodic chamber by gas chromatography.

Definition of Performance Parameters. EQE corresponds to the percentage of incident photons converted to electrons at a selected bias and was calculated using

$$\mathrm{EQE}(\%) = \frac{123.98J(\mu\mathrm{A/cm^2})}{[\lambda(\mathrm{nm})][I(\mathrm{mW/cm^2})]} \quad (1)$$

with current density (J), irradiation wavelength (λ), and light intensity (I).

The faradaic yield was calculated based on the ratio of measured gaseous product versus the amount of theoretically expected product based on accumulated charge during CPE (two electrons consumed per molecule of H_2 and four electrons per molecule of O_2). The TOF of PSII for O_2 production, assuming 100% faradaic yield, has been determined from the photocurrent (I_{Ph}), moles of adsorbed PSII (n), number of electrons (e), and the Avogadro number (N_A):

$$\mathrm{TOF} = \frac{I_{Ph}}{4eN_An} \quad (2)$$

The overall light-to-hydrogen conversion efficiency (η) was calculated using[1]

$$\eta(\%) = \frac{[J(\mu\mathrm{A/cm^2})][1.23 - U(\mathrm{V})]}{10[I(\mathrm{mW/cm^2})]} \quad (3)$$

with current density (J), applied voltage (U), and light intensity (I).

■ ASSOCIATED CONTENT

Supporting Information

Supporting Figures S1–S10. The Supporting Information is available free of charge on the ACS Publications website at DOI: 10.1021/jacs.5b03737.

■ AUTHOR INFORMATION

Corresponding Author

*reisner@ch.cam.ac.uk

Notes

The authors declare no competing financial interest.

■ ACKNOWLEDGMENTS

This work was supported by the U.K. Engineering and Physical Sciences Research Council (EP/H00338X/2 to E.R. and EP/G037221/1, nanoDTC, to D.M.), the U.K. Biology and Biotechnological Sciences Research Council (BB/K002627/1 to A.W.R. and BB/K010220/1 to E.R.), a Marie Curie Intra-European Fellowship (PIEF-GA-2013-625034 to C.-Y.L.), a Marie Curie International Incoming Fellowship (PIIF-GA-2012-328085 RPSII to J.J.Z.), and the CEA and the CNRS (to J.C.F.-C.). A.W.R. holds a Wolfson Merit Award from the Royal Society. We would also like to thank Dr. Sumeet Mahajan for his support in the early stage of this project, Dr. Christine Cavazza for providing us with *D. baculatum* [NiFeSe]-hydrogenase, Mrs. Yi-Hsuan Lai for conducting XRD measurements, Mr. David Evans for help in preparing the artwork in Figure 1, and Dr. Hyun S. Park, Dr. Andrea Fantuzzi, and Mr. Nicholas Paul for valuable discussions.

■ REFERENCES

(1) Walter, M. G.; Warren, E. L.; McKone, J. R.; Boettcher, S. W.; Mi, Q.; Santori, E. A.; Lewis, N. S. *Chem. Rev.* **2010**, *110*, 6446–6473.
(2) Reece, S. Y.; Hamel, J. A.; Sung, K.; Jarvi, T. D.; Esswein, A. J.; Pijpers, J. J. H.; Nocera, D. G. *Science* **2011**, *334*, 645–648.
(3) Warren, S. C.; Voïtchovsky, K.; Dotan, H.; Leroy, C. M.; Cornuz, M.; Stellacci, F.; Hébert, C.; Rothschild, A.; Grätzel, M. *Nat. Mater.* **2013**, *12*, 842–849.
(4) Nelson, N.; Ben-Shem, A. *Nat. Rev. Mol. Cell Biol.* **2004**, *5*, 971–982.
(5) Blankenship, R. E.; Tiede, D. M.; Barber, J.; Brudvig, G. W.; Fleming, G.; Ghirardi, M.; Gunner, M. R.; Junge, W.; Kramer, D. M.; Melis, A.; Moore, T. A.; Moser, C. C.; Nocera, D. G.; Nozik, A. J.; Ort, D. R.; Parson, W. W.; Prince, R. C.; Sayre, R. T. *Science* **2011**, *332*, 805–809.
(6) Andersson, I.; Backlund, A. *Plant Physiol. Biochem.* **2008**, *46*, 275–291.
(7) Kato, M.; Zhang, J. Z.; Paul, N.; Reisner, E. *Chem. Soc. Rev.* **2014**, *43*, 6485–6497.
(8) Vinyard, D. J.; Ananyev, G. M.; Dismukes, G. C. *Annu. Rev. Biochem.* **2013**, *82*, 577–606.
(9) Grundmeier, A.; Dau, H. *Biochim. Biophys. Acta, Bioenerg.* **2012**, *1817*, 88–105.
(10) Lubitz, W.; Ogata, H.; Rüdiger, O.; Reijerse, E. *Chem. Rev.* **2014**, *114*, 4081–4148.
(11) Jones, A. K.; Sillery, E.; Albracht, S. P. J.; Armstrong, F. A. *Chem. Commun.* **2002**, 866–867.
(12) Melis, A. *Energy Environ. Sci.* **2012**, *5*, 5531–5539.
(13) Dubini, A.; Ghirardi, M. L. *Photosynth. Res.* **2015**, *123*, 241–253.
(14) Volgusheva, A.; Styring, S.; Mamedov, F. *Proc. Natl. Acad. Sci. U. S. A.* **2013**, *110*, 7223–7228.
(15) Michel, H. *Angew. Chem., Int. Ed.* **2012**, *51*, 2516–2518.
(16) Umena, Y.; Kawakami, K.; Shen, J.-R.; Kamiya, N. *Nature* **2011**, *473*, 55–60.
(17) Garcin, E.; Vernede, X.; Hatchikian, E. C.; Volbeda, A.; Frey, M.; Fontecilla-Camps, J. C. *Structure* **1999**, *7*, 557–566.
(18) Liu, Y. J.; Štefanić, G.; Rathouský, J.; Hayden, O.; Bein, T.; Fattakhova-Rohlfing, D. *Chem. Sci.* **2012**, *3*, 2367–2374.
(19) Koenderink, A. F.; Lagendijk, A.; Vos, W. L. *Phys. Rev. B* **2005**, *72*, 153102.
(20) Badura, A.; Guschin, D.; Esper, B.; Kothe, T.; Neugebauer, S.; Schuhmann, W.; Rögner, M. *Electroanalysis* **2008**, *20*, 1043–1047.
(21) Kato, M.; Cardona, T.; Rutherford, A. W.; Reisner, E. *J. Am. Chem. Soc.* **2012**, *134*, 8332–8335.
(22) Armstrong, F. A.; Belsey, N. A.; Cracknell, J. A.; Goldet, G.; Parkin, A.; Reisner, E.; Vincent, K. A.; Wait, A. F. *Chem. Soc. Rev.* **2009**, *38*, 36–51.
(23) Goldet, G.; Wait, A. F.; Cracknell, J. A.; Vincent, K. A.; Ludwig, M.; Lenz, O.; Friedrich, B.; Armstrong, F. A. *J. Am. Chem. Soc.* **2008**, *130*, 11106–11113.
(24) Blanco, A.; Chomski, E.; Grabtchak, S.; Ibisate, M.; John, S.; Leonard, S. W.; Lopez, C.; Meseguer, F.; Miguez, H.; Mondia, J. P.; Ozin, G. A.; Toader, O.; van Driel, H. M. *Nature* **2000**, *405*, 437–440.
(25) Zakhidov, A. A.; Baughman, R. H.; Iqbal, Z.; Cui, C.; Khayrullin, I.; Dantas, S. O.; Marti, J.; Ralchenko, V. G. *Science* **1998**, *282*, 897–901.

DOI: 10.1021/jacs.5b03737
J. Am. Chem. Soc. 2015, 137, 8541–8549

(26) Yablonovitch, E. *J. Opt. Soc. Am. B* **1993**, *10*, 283−295.
(27) Diguna, L. J.; Shen, Q.; Kobayashi, J.; Toyoda, T. *Appl. Phys. Lett.* **2007**, *91*, 023116.
(28) Schaming, D.; Renault, C.; Tucker, R. T.; Lau-Truong, S.; Aubard, J.; Brett, M. J.; Balland, V.; Limoges, B. *Langmuir* **2012**, *28*, 14065−14072.
(29) Liu, Y.; Peters, K.; Mandlmeier, B.; Müller, A.; Fominykh, K.; Rathousky, J.; Scheu, C.; Fattakhova-Rohlfing, D. *Electrochim. Acta* **2014**, *140*, 108−115.
(30) Arsenault, E.; Soheilnia, N.; Ozin, G. A. *ACS Nano* **2011**, *5*, 2984−2988.
(31) Renault, C.; Andrieux, C. P.; Tucker, R. T.; Brett, M. J.; Balland, V.; Limoges, B. *J. Am. Chem. Soc.* **2012**, *134*, 6834−6845.
(32) Sugiura, M.; Inoue, Y. *Plant Cell Physiol.* **1999**, *40*, 1219−1231.
(33) Renger, G.; Renger, T. *Photosynth. Res.* **2008**, *98*, 53−80.
(34) Bachmeier, A.; Armstrong, F. *Curr. Opin. Chem. Biol.* **2015**, *25*, 141−151.
(35) Parkin, A.; Goldet, G.; Cavazza, C.; Fontecilla-Camps, J. C.; Armstrong, F. A. *J. Am. Chem. Soc.* **2008**, *130*, 13410−13416.
(36) Sakai, T.; Mersch, D.; Reisner, E. *Angew. Chem., Int. Ed.* **2013**, *52*, 12313−12316.
(37) Vincent, K. A.; Parkin, A.; Armstrong, F. A. *Chem. Rev.* **2007**, *107*, 4366−4413.
(38) Reisner, E.; Powell, D. J.; Cavazza, C.; Fontecilla-Camps, J. C.; Armstrong, F. A. *J. Am. Chem. Soc.* **2009**, *131*, 18457−18466.
(39) Muresan, N. M.; Willkomm, J.; Mersch, D.; Vaynzof, Y.; Reisner, E. *Angew. Chem., Int. Ed.* **2012**, *51*, 12749−12753.
(40) de Poulpiquet, A.; Marques-Knopf, H.; Wernert, V.; Giudici-Orticoni, M. T.; Gadiou, R.; Lojou, E. *Phys. Chem. Chem. Phys.* **2014**, *16*, 1366−1378.
(41) Krishnan, S.; Armstrong, F. A. *Chem. Sci.* **2012**, *3*, 1015−1023.
(42) Cracknell, J. A.; Vincent, K. A.; Armstrong, F. A. *Chem. Rev.* **2008**, *108*, 2439−2461.
(43) Hambourger, M.; Gervaldo, M.; Svedruzic, D.; King, P. W.; Gust, D.; Ghirardi, M.; Moore, A. L.; Moore, T. A. *J. Am. Chem. Soc.* **2008**, *130*, 2015−2022.
(44) Rüdiger, O.; Abad, J. M.; Hatchikian, E. C.; Fernandez, V. M.; De Lacey, A. L. *J. Am. Chem. Soc.* **2005**, *127*, 16008−16009.
(45) Svedružić, D.; Blackburn, J. L.; Tenent, R. C.; Rocha, J.-D. R.; Vinzant, T. B.; Heben, M. J.; King, P. W. *J. Am. Chem. Soc.* **2011**, *133*, 4299−4306.
(46) Ulas, G.; Brudvig, G. W. *J. Am. Chem. Soc.* **2011**, *133*, 13260−13263.
(47) Vincent, K. A.; Cracknell, J. A.; Lenz, O.; Zebger, I.; Friedrich, B.; Armstrong, F. A. *Proc. Natl. Acad. Sci. U. S. A.* **2005**, *102*, 16951−16954.
(48) Lazarus, O.; Woolerton, T. W.; Parkin, A.; Lukey, M. J.; Reisner, E.; Seravalli, J.; Pierce, E.; Ragsdale, S. W.; Sargent, F.; Armstrong, F. A. *J. Am. Chem. Soc.* **2009**, *131*, 14154−14155.
(49) Kothe, T.; Plumeré, N.; Badura, A.; Nowaczyk, M. M.; Guschin, D. A.; Rögner, M.; Schuhmann, W. *Angew. Chem., Int. Ed.* **2013**, *52*, 14233−14236.
(50) Wilker, M. B.; Shinopoulos, K. E.; Brown, K. A.; Mulder, D. W.; King, P. W.; Dukovic, G. *J. Am. Chem. Soc.* **2014**, *136*, 4316−4324.
(51) Caputo, C. A.; Gross, M. A.; Lau, V. W.; Cavazza, C.; Lotsch, B. V.; Reisner, E. *Angew. Chem., Int. Ed.* **2014**, *53*, 11538−11542.
(52) Hatchikian, E. C.; Bruschi, M.; Le Gall, J. *Biochem. Biophys. Res. Commun.* **1978**, *82*, 451−461.
(53) Sedoud, A.; Kastner, L.; Cox, N.; El-Alaoui, S.; Kirilovsky, D.; Rutherford, A. W. *Biochim. Biophys. Acta, Bioenerg.* **2011**, *1807*, 216−226.

DOI: 10.1021/jacs.5b03737
J. Am. Chem. Soc. 2015, 137, 8541−8549